



Published in final edited form as:

Biochemistry. 2008 August 5; 47(31): 8080–8093. doi:10.1021/bi8007356.

X-ray crystallographic and Solution State NMR Spectroscopic Investigations of NADP⁺ Binding to Ferredoxin-NADP Reductase (FPR) from *Pseudomonas aeruginosa*^{†,‡}

An Wang[§], Juan Carlos Rodríguez[§], Huijong Han[£], Ernst Schönbrunn[£], and Mario Rivera^{§,*}

[§]Ralph N. Adams Institute for Bioanalytical Chemistry & Department of Chemistry, University of Kansas, Multidisciplinary Research Building, 2030 Becker Dr., Room 220 E, Lawrence, KS 66047

[£]Moffitt Cancer Center, 12902 Magnolia Drive, Tampa, FL 33612

Abstract

The ferredoxin nicotinamide adenine dinucleotide phosphate reductase from *Pseudomonas aeruginosa* (*pa*-FPR) in complex with NADP⁺ has been characterized by X-ray crystallography and in solution by NMR spectroscopy. The structure of the complex revealed that *pa*-FPR harbors a pre-formed NADP⁺ binding pocket where the cofactor binds with minimal structural perturbation of the enzyme. These findings were complemented by obtaining sequential backbone resonance assignments of this 29,518 kDa enzyme, which enabled the study of the *pa*-FPR-NADP complex by monitoring chemical shift perturbations induced by addition of NADP⁺ or the inhibitor, adenine dinucleotide phosphate (ADP), to *pa*-FPR. The results are consistent with a pre-formed NADP⁺ binding site and also demonstrate that the *pa*-FPR-NADP complex is largely stabilized by interactions between the protein and the 2'P AMP portion of the cofactor. Analysis of the crystal

[†]This work was supported by a grant from the National Institute of Health, GM-50503 (M.R.)

[‡]Coordinates for the structure of *pa*-FPR-NADP have been deposited in the protein data bank under accession code 3CRZ. Backbone resonance assignments for *pa*-FPR have been deposited in the BMRB under access code 15788

*To whom correspondence should be addressed. Ralph N. Adams Institute for Bioanalytical Chemistry & Department of Chemistry, University of Kansas, Multidisciplinary Research Building, 2030 Becker Dr., Room 220 E, Lawrence, Kansas 66047. Phone: 785-864-4936. Fax: 785-864-5396. mrivera@ku.edu

¹Abbreviations:

P. aeruginosa *Pseudomonas aeruginosa*

A. vinelandii *Azotobacter vinelandii*

R. capsulatus *Rhodobacter capsulatus*

P. pastoris *Pichia pastoris*

FNR ferredoxin NADP⁺ reductase

***pa*-FPR** *Pseudomonas aeruginosa* ferredoxin nicotinamide adenine dinucleotide phosphate reductase

***Av*-FPR** *Azotobacter vinelandii* ferredoxin reductase

FAD flavin adenine dinucleotide

NAD(P)H nicotinamide adenine dinucleotide (phosphate)

adenosine 2',5'-(AMP) phosphate

IPTG isopropyl-1-thiol-D-galactopyranoside

DTT dithiothreitol

structure also shows a vast network of interactions between the two cofactors, FAD and NADP⁺, and the characteristic AFVEK²⁵⁸ C'-terminal extension that is typical of bacterial FPRs but is absent in their plastidic ferredoxin NADP⁺ reductase (FNR) counterparts. The conformations of NADP⁺ and FAD in *pa*-FPR place their respective nicotinamide and isoalloxazine rings 15 Å apart and separated by residues in the C'-terminal extension. The network of interactions between NADP⁺, FAD and residues in the C'-terminal extension indicate that the gross conformational rearrangement that would be necessary to place the nicotinamide and isoalloxazine rings parallel and adjacent to one another for direct hydride transfer between NADPH and FAD in *pa*-FPR is highly unlikely. This conclusion is supported by observations made in the NMR spectra of *pa*-FPR and *pa*-FPR-NADP, which strongly suggest that residues in the C'-terminal sequence do not undergo conformational exchange in the presence or in the absence of NADP⁺. These findings are discussed in the context of a possible stepwise electron-proton-electron transfer of hydride in the oxidation of NADPH by FPR enzymes.

Ferredoxin NADP⁺ reductases (FNRs), which catalyze the reversible electron transfer between NADP(H) and their cognate ferredoxin or flavodoxin partners, are found in plastids, phototrophic and heterotrophic bacteria and in mitochondria (1). One of the best characterized enzymes is FNR from spinach leaves, a typical FNR found in plastids, which utilizes the reducing power of electromagnetic radiation to reduce NADP⁺ and produce the NADPH needed for subsequent photosynthetic paths (2). In contrast, bacterial ferredoxin reductases oxidize the NADPH pool, in order to use this reducing potential in a large number of oxidoreductive processes. For instance, *E. coli* flavodoxin reductase functions in the reduction of flavodoxin for the activation of anaerobic enzymes and in the oxidation of NADPH as a mechanism of protection against oxidative stress (3-5). In *R. capsulatus* (5), *A. vinelandii* (4) and *E. coli* (3) the gene *fpr* encodes a ferredoxin (flavodoxin) nicotinamide adenine dinucleotide phosphate reductase (FPR) that functions in the oxidation of NADPH as a mechanism of defense against oxidative stress. A similar FPR in *P. aeruginosa* (*pa*-FPR) has been characterized as a 258-residue long NADPH-dependent enzyme that uses FAD as cofactor (6). Although it is possible that *pa*-FPR also functions in mitigating oxidative stress (4), it has been shown that under iron starvation conditions it functions by shuttling electrons from NADPH to a heme oxygenase, thus supporting the process of releasing iron from exogenously acquired heme for subsequent metabolic use (6).

The crystal structure of *pa*-FPR (6) revealed a fold very similar that characteristic of the FNR superfamily and is almost identical to the structure of FPR from *A. vinelandii* (*Av*-FPR) (7), *R. capsulatus* (8) and *E. coli* flavodoxin reductase (9). Comparative analysis of the X-ray crystal structures of ferredoxin reductases uncovered some interesting differences in the context of a similar fold. These differences led to the classification of these enzymes into reductases of the plastidic class, *i.e.*, enzymes from chloroplasts and cyanobacteria, and enzymes of the bacterial class, which are further subdivided into proteobacteria subclass I enzymes (*A. vinelandii*, *R. capsulatus*, *P. aeruginosa*) and proteobacteria subclass II reductases (*E. coli* flavodoxin reductase) (10). The structures showed that plastidic FNRs and bacterial FPRs differ in the conformation and chemical environment of the FAD cofactor. In the plastidic enzymes the FAD is bound in an extended conformation, which is stabilized by specific interactions with residues in a sheet-loop-sheet motif (green in Figure 1-A). These encompass π -stacking of the adenine ring with the conserved aromatic side chain of Tyr120 and hydrogen bonding interactions involving the 2'-P AMP moiety. In comparison, bacterial FPRs lack the sheet-loop-sheet motif that stabilizes the extended FAD conformation, thus the cofactor adopts a folded conformation, where the adenine ring π -stacks with the conserved aromatic side chain of residue 255 (Figure 1-B). The FMN portion of FAD in plastidic and bacterial reductases exhibit very similar conformations and chemical environments. Additional important differences occur in the carboxyl terminal domains, which are typically thought to be involved

in NADP(H) binding. Whereas in plastidic FNRs the carboxyl terminal Tyr (Y314 in spinach FNR, Y308 in pea FNR and Y303 in *Anabaena* FNR) π -stacks against the isoalloxazine ring of FAD (11,12) (see Figure 1-A), in subclass I bacterial FPRs this residue is replaced by Ala254, which is followed by a FVEK²⁵⁸ terminal sequence (Figure 1-B). In the structures of *pa*-FPR and *Av*-FPR the carbonyl oxygen of Ala254 packs against the isoalloxazine ring, replacing the conserved π -stacking interaction between the carboxyl terminal Tyr ring and the isoalloxazine ring seen in plastidic FNRs. In subclass II bacterial enzymes, a conserved terminal Trp is found immediately after the position occupied by the terminal Tyr in plastidic enzymes, thus extending the carboxy terminal domain by only one residue. In these enzymes FAD also adopts a folded conformation.

The binding of NADP⁺ to FNRs has been the subject of intense investigations. Cocrystallization of *Anabaena* FNR (13) with NADP⁺ revealed a complex in which the 2'P AMP portion of the cofactor is stabilized in a manner similar that observed in the NADP⁺ complex obtained by soaking crystals of the *Anabaena* enzyme in NADP⁺ solution (14). The conformation of the nicotinamide portion of the cofactor, however, is clearly distinct in the two structures. In the structure of *Anabaena* FNR obtained from crystals soaked in NADP⁺ solutions the nicotinamide ring extends toward the surface of the protein and away from the isoalloxazine ring, whereas in the structure obtained from co-crystallization with NADP⁺, the side chain of the carboxyl terminal Tyr (Y303) is stacked between the nicotinamide and isoalloxazine rings. The latter structure resembles more the “productive” interactions seen in other flavoenzyme families that are structurally and functionally different from FNRs (*i.e.* glutathione reductase) where the nicotinamide and isoalloxazine rings stack parallel and adjacent to one another (15,16). Nevertheless, the side chain of Tyr303 is not displaced to allow direct overlap of the cofactor rings, as would be expected in a “productive” complex that facilitates direct hydride transfer. A “productive” complex was observed only in Y308 mutants (the C'-terminal residue) of pea-FNR, where the NADP⁺ nicotinamide ring is nearly parallel and adjacent to the FAD isoalloxazine ring (17).

These observations have led to the conclusion that NADP⁺ binding to FNRs is a two-step process (17). In the first step the 2'-P-AMP moiety binds tightly and anchors the cofactor, whereas the nicotinamide portion is disordered. In the second step, the enzyme-cofactor complex is expected to sample a set of “productive” conformations in which the side chain of the C'-terminal Tyr is displaced, thus allowing overlap of the nicotinamide and isoalloxazine rings to facilitate hydride transfer. In the context of this mechanism, it is significant that in the structures of FPRs from *A. vinelandii*, *R. capsulatus* and *P. aeruginosa* the terminal Tyr is replaced by Ala254, which is followed by a C'-terminal extension (AFVEK²⁵⁸). This extension of the sequence, in principle, can be expected to slow the rate of conformational rearrangements needed to access the “productive” conformation of cofactors thought to facilitate direct hydride transfer, assuming that the binding of NADP⁺ is similar in FNRs and FPRs. Nevertheless, nothing is known about the structural properties of the NADP(H) complex of FPRs, and the functional role, if any, played by the C'-terminal extension characteristic of these enzymes has so far been elusive. In this report we present the X-ray crystal structure of the *pa*-FPR-NADP complex, which shows an extensive network of interactions between FAD, NADP⁺ and the C'-terminal extension. Complementary observations made with the aid of NMR spectroscopy in solution support the notion inferred from analysis of the network of interactions in the crystal structure that the C'-terminal tail is not dynamically active, even upon NADP⁺ binding. These findings, which suggest that the C'-terminal extension will likely not be readily displaced to allow “productive” packing of the isoalloxazine and nicotinamide rings for direct hydride transfer, are discussed in the context of a possible multistep hydride transfer operative in the oxidation of NADPH by FPR enzymes.

EXPERIMENTAL SECTION

Expression of labeled *pa*-FPR for NMR Studies

pa-FPR was expressed and purified following previously reported protocols (6). For the expression of ^{15}N labeled *pa*-FPR 1.0 L-cultures were incubated at 37 °C in medium containing non-labeled nutrients. Upon reaching mid-log phase the cells were centrifuged and transferred to the same volume of fresh minimum medium containing labeled $^{15}\text{NH}_4\text{Cl}$ (1.0 g/L) and cultured to an optical density at 600 nm (OD_{600}) of approximately 0.7. The culture was then transferred to a shaker incubator pre-equilibrated at 10 °C where the cells were cultured for 30 min to allow thermal equilibrium. Protein expression was then induced by addition of IPTG (0.3 mM final concentration), followed by culturing at 10 °C for approximately 14 h before harvesting by centrifugation. Uniformly ^{13}C and ^{15}N -labeled *pa*-FPR, [$\text{U-}^{13}\text{C}$, ^{15}N]-*pa*-FPR, was expressed in a similar manner, except that cells centrifuged after reaching mid-log phase were resuspended in minimal medium containing $^{15}\text{NH}_4\text{Cl}$ (1.0 g/L) and $^{13}\text{C}_6\text{-D-glucose}$ (2.0 g/L). Prior to expression, the ArcticExpress™ RIL cells harboring the recombinant plasmid containing the *pa-fpr* gene were adapted to grow in D_2O using a protocol similar to that reported for the expression of deuterated proteins in *P. pastoris* (18). In short, cells were plated on an LB-ampicillin plate and grown at 37 °C for 16 h. An isolated colony from this plate was transferred to 10 mL of LB-ampicillin medium containing 25% D_2O (v/v) and the cells grown at 37 °C overnight. The resultant cell suspension was used to plate LB-agar containing 25% D_2O and the cells were grown at 37 °C for 16 h. An isolated colony from this plate was transferred to 10 mL of LB-Amp medium (50% D_2O v/v) to start a new cycle of adaptation. Subsequent cycles were carried out similarly and included adaptation at 75% and 95 % D_2O . Cells grown in 95% D_2O were used to make a glycerol stab culture stock. A single colony of cells grown in an LB-amp plate made with 95% D_2O was transferred to 10 mL of LB-Amp (99.9% D_2O) and cultured at 37 °C and 220 rpm overnight. This culture was used to inoculate 100 mL (99.9% D_2O) M9 medium containing $^{15}\text{NH}_4\text{Cl}$ (1.0 g/L) and $^{13}\text{C}_6\text{-D-glucose}$ (2.0 g/L) and the cells were grown at 37 °C to an OD_{600} of ~ 0.7. Fifty mL from this culture were used to inoculate 1.0 L of M9 medium (99.9% D_2O) containing $^{15}\text{NH}_4\text{Cl}$ (1.0 g/L) and $^{13}\text{C}_6\text{-D-glucose}$ (2.0 g/L), and the cells grown to an OD_{600} of ~ 0.7 at 37 °C. The culture was then equilibrated at 10 °C, followed by induction of protein expression by the addition of IPTG (0.2 mM final concentration) and culturing at 10 °C for 30 h. Cell harvesting, cell lysis and enzyme purification were carried out as described previously (6). Amide and side chain deuterons were exchanged for hydrogen as follows: Pure protein was dissolved in 50 mM sodium phosphate buffer (pH 7.0) containing 8 M urea, 100 mM NaCl, and 0.1 mM FAD to a final concentration of ~ 8 μM and incubated at 37 °C for 3 h. This solution was dialyzed extensively against 50 mM sodium phosphate (pH 7.0) containing 100 mM NaCl, 10% (v/v) glycerol, 0.1 mM EDTA, and 5 mM DTT at 4°C. The resultant solution was concentrated by ultrafiltration (Centricon -10, MW cutoff 10 kDa) to 1.0 mL and loaded onto a Sephadex G-50 column (100 × 1.6 cm) to remove free FAD and eluted with 50 mM sodium phosphate buffer (pH 7.0).

Selective amino acid labeling of *pa*-FPR was carried out following a protocol reported previously (19) with some modifications (20). The minimal medium used to obtain uniformly labeled protein was supplemented with the following amino acids (g/L) : *L*-Ala (0.5), *L*-Arg (0.4), *L*-Asp (0.4), *L*-Asn (0.4), *L*-Cys (0.05), *L*-Gln (0.4), *L*-Glu (0.65), Gly (0.55), *L*-His (0.1), *L*-Ile (0.23), *L*-Leu (0.23), *L*-Lys hydrochloride (0.42), *L*-Met (0.25), *L*-Phe (0.13), *L*-Pro (0.1), *L*-Ser (2.10), *L*-Thr (0.23), *L*-Tyr (0.17), *L*-Val (0.23), and *L*-Trp (0.05). All amino acids except *L*-Trp and the ^{15}N -enriched amino acid were added in solid form to the media prior to autoclaving. ^{15}N -Trp was filter sterilized and added prior to inoculation. For the preparation of [^{15}N -Leu]-*pa*-FPR, 10 mL of LB medium was inoculated with a single colony and grown overnight at 37 °C. The overnight culture was used to inoculate 1.0 L of M9 medium supplemented as above, but not containing *L*-Leu. The cells were grown at 37 °C to an

OD₆₀₀ of ~ 0.7, equilibrated at 10 °C and supplemented with ¹⁵N-*L*-Leu previous to induction of protein expression by the addition of IPTG (of 0.2 mM final concentration) and cultured for 12–15 h. The same process was used to prepare *pa*-FPR labeled selectively with ¹⁵N-Val, ¹⁵N-Glu, ¹⁵N-Phe and ¹⁵N-Asp. A slight modification was needed to prepare enzyme labeled with ¹⁵N-Tyr, ¹⁵N-Phe and ¹⁵N-Thr. In the preparation of [¹⁵N-Tyr]-*pa*-FPR and [¹⁵N-Phe]-*pa*-FPR, 0.25 g of glyphosate (N-phosphonomethyl-glycine) was added together with the ¹⁵N-labeled amino acid. In the preparation of [¹⁵N-Thr]-*pa*-FPR, additional 0.23 g/L of *L*-Ile and 0.115 g/L of *L*-Val were added together with the ¹⁵N-Thr to minimize isotope scrambling to Ile or Val. In the preparation of [¹⁵N-Gly]-*pa*-FPR, the relatively minor scrambling from ¹⁵N-Gly to ¹⁵N-Ser was intentionally preserved because it was useful in the identification of cross-peaks originating from Ser residues in *pa*-FPR. Cell harvesting, cell lysis and enzyme purification were carried out as described previously (6).

NMR Sample Preparation

Protein concentrations were determined by measuring the absorption of *pa*-FPR solutions at 450 nm ($\epsilon_{450} = 11.5 \text{ mM}^{-1} \text{ cm}^{-1}$) (6). NMR samples typically contained 0.1 – 1.2 mM *pa*-FPR, 5 – 10 % D₂O in 50 mM sodium phosphate buffer (pH = 7.0). The details of experimental conditions used for specific NMR experiments are shown in the appropriate figure captions.

NMR Spectroscopy and Backbone Resonance Assignments

NMR experiments were carried out in a Bruker Avance 800 spectrometer equipped with a 5 mm TXI ¹H-¹³C/¹⁵N/D_{xyz} gradient probe. Two- and three-dimensional NMR experiments (¹H-¹⁵N-HSQC, ¹H-¹⁵N-TROSY-HSQC, HNCA, HN(CO)CA, TROSY-HNCACB, TROSY-HN(CO)CACB, TROSY-HN(CA)CO, and TROSY-HNCO) for NMR assignment were carried out at 25 °C. Amino acid selective ¹⁵N-labeled *pa*-FPR: [¹⁵N-Gly]-*pa*-FPR, [¹⁵N-Leu]-*pa*-FPR, [¹⁵N-Val]-*pa*-FPR, [¹⁵N-Glu]-*pa*-FPR, [¹⁵N-Phe]-*pa*-FPR, [¹⁵N-Asp]-*pa*-FPR, [¹⁵N-Tyr]-*pa*-FPR and [¹⁵N-Thr]-*pa*-FPR were used to acquire ¹H-¹⁵N HSQC spectra. Two- and three-dimensional NMR spectra were processed using NMRPipe and analyzed with Sparky. ¹H chemical shifts were referenced to the proton resonance of DSS at 0 ppm, while ¹⁵N and ¹³C shifts were referenced indirectly using the ratios 0.101329118 and 0.251449530, respectively (21).

Chemical Shift Perturbation Experiments

¹H-¹⁵N HSQC spectra were recorded at 25 °C using Varian Unity Inova 600 MHz and Bruker Avance 800 MHz spectrometers. [¹⁵N]-*pa*-FPR (500 μ L, 0.25 mM) in 50 mM sodium phosphate (pH 7.0, 10 % D₂O) contained in a 5 mm diameter NMR tube was titrated with a stock solution of NADP⁺ (39 mM) dissolved in the same buffer. Titrations were carried out by addition of 0.05, 0.10, 0.20, 0.30, 0.40, 0.50, 0.75, 1.0, 1.5, 2.0, 3.5, 5.0, 7.5, 10, 15, 20 and 25 equivalents of NADP⁺ relative to *pa*-FPR. The pH of the solution after the addition of each aliquot of NADP⁺ was adjusted to 7.0 prior to recording the corresponding ¹H-¹⁵N HSQC spectrum. The spectra were acquired at 25 °C using Varian Unity Inova 600 MHz. The data were processed using NMRpipe and analyzed using Sparky. Similar experiments were carried out with adenosine 2'5'-diphosphate (ADP), a competitive inhibitor of ferredoxin reductase enzymes.

X-ray crystallography

X-ray-quality single crystals of *pa*-FPR in complex with NADP⁺ were grown using the hanging drop vapor diffusion method by mixing 2 μ L of *pa*-FPR (20 mg/mL) dissolved in 20 mM Tris (pH 7.6) containing 10 mM NADP⁺ with 2 μ L of a solution consisting of 200 mM ammonium acetate, 100 mM sodium citrate tribasic dihydrate and 25% PEG-4000 (pH 5.6). Diffraction data were recorded at –180 °C using the rotation method on a single flash-frozen crystal

[Detector: R-axis IV⁺⁺ image plate; X-rays: CuK α , focused by mirror optics; Generator: Rigaku RU300 (MSC, The Woodlands, TX, USA)]. The cryoprotectant was 20 % ethylene glycol. X-ray data were reduced with XDS (22); the program package CNS (23) was employed for phasing and refinement; model building was performed with O (24). The structure was solved by molecular replacement using the coordinates of ferredoxin oxidoreductase from *pa*-FPR (PDB entry 2QDX) as search model, stripped of solvent molecules and ligands. Refinement was performed using data to the highest resolution with no sigma cut-off applied. Several rounds of minimization simulated annealing (2500 K starting temperature) and restrained individual B-factor refinement were carried out. Data collection and refinement statistics are summarized in Table 1.

RESULTS AND DISCUSSION

Precedents guiding current views of hydride transfer between flavin and nicotinamide are grounded on observations made with the structure of glutathione reductase, a flavoenzyme that is functionally and structurally different from FNR (15,16). The structure of glutathione reductase shows the nicotinamide ring parallel and adjacent to the isoalloxazine ring; this relative orientation, which likely facilitates direct hydride ion transfer, is viewed as a “productive” complex. In the structures of plastidic FNRs, however, the side chain of the C'-terminal Tyr lies parallel to the flavin isoalloxazine ring, thus occupying the place that would be taken by the nicotinamide ring in a “productive” complex. Work aimed at explaining these structural observations led to the hypothesis that NADP⁺ binding to plastidic FNRs is a two step process; with the first step involving strong interactions between the 2' adenosyl phosphate moiety and FNR, whereas the nicotinamide portion undergoes less specific interactions with the enzyme. In the second step the side chain of the terminal Tyr moves and allows the nicotinamide ring to stack parallel to the isoalloxazine ring, thus forming a transient but “productive” complex conducive to direct hydride transfer (17).

In comparison, previous to this report, virtually nothing was known regarding the binding of NADP⁺ to bacterial FPRs. Amino acid sequence alignments and the structures of *Av*- and *pa*-FPRs had demonstrated that the position occupied by the terminal Tyr in FNRs is occupied by Ala in the bacterial enzymes (A254 in *pa*-FPR), where the carbonyl oxygen of this residue stacks against the isoalloxazine ring of FAD (6,7). In addition, FPR enzymes possess a characteristic C'-terminal extension following A254 (AFVEK²⁵⁸). The effect of NADP⁺ binding on the interaction between A254 and FAD and on the conformation of the C'-terminal extension, however, was difficult to predict. The structure of the *pa*-FPR-NADP complex reported herein provides a first view of the interactions between NADP⁺ and *pa*-FPR. As will be shown below, analysis of the structure shows a vast network of stabilizing interactions between FAD, NADP⁺ and the C'-terminal extension, which suggests that the gross conformational rearrangements that would be needed for placing the nicotinamide and isoalloxazine rings parallel and adjacent is not likely to occur. These observations are discussed in the context of a putative mechanism where the oxidation of NADPH by FPRs may occur via a stepwise rather than direct hydride transfer.

The Crystal Structure of *pa*-FPR-NADP shows a network of interactions encompassing FAD, NADP⁺ and the C'-Terminal Extension

The recently reported crystal structure of *pa*-FPR (6) showed that the enzyme folds into a two-domain structure, typical of the ferredoxin NADP⁺ reductase superfamily. The FAD cofactor binds in the N-terminal domain (residues 1–87), comprised of an antiparallel β -barrel (β 1– β 6) capped by helix α 1. The stabilizing interactions between FAD and *pa*-FPR have been described in detail (6); these interactions remain largely unchanged in the structure of the *pa*-FPR-NADP complex, which shows that NADP⁺ binds in the C'-terminal domain of the β -sheet, comprised

of $\beta 7$, $\beta 10$, the loop connecting $\beta 7$ to $\alpha 3$, the N-terminal residues of $\alpha 3$ and the carboxy terminal residues AFVEK²⁵⁸ (Figure 2). There are several stabilizing interactions between the polypeptide and the cofactor (Figure 3): Starting at the adenine end of the NADP⁺ molecule, the NH₂ nitrogen in this ring is within hydrogen bonding distance of the hydroxyl oxygen in Ser223 and the carboxylate group of Glu227. The 2'-phosphate (2'-P) is anchored to the enzyme via H-bonds and salt bridges to the hydroxyl oxygen of Thr181, the guanidinium NH and NH₂⁺ groups in the side chain of Arg182 and the guanidinium NH group of Arg190. A salt bridge between the negatively charged oxygen in the pyrophosphate P1 group of NADP⁺ and the guanidinium NH₂⁺ group of Arg145, and a hydrogen bond between the NH group of the same side chain and the neutral oxygen in P1 stabilize this portion of the cofactor. The 1'- and 2'-hydroxyl groups in the nicotinamide ribose ring of NADP⁺ are engaged in hydrogen bonding interactions with the adenine 3N atom and with the ribose 2-hydroxyl groups of FAD, respectively. It is important to point out that despite the proximity suggested by these interactions, the isoalloxazine and nicotinamide rings of FAD and NADP⁺ are separated by the C'-terminal residues. This network is expanded by π -stacking interactions between the adenine ring in FAD and the aromatic side chain of Phe255; the latter is also T-stacked against the nicotinamide ring of NADP⁺. The nicotinamide amide NH and carbonyl groups are within hydrogen bonding distance of the carboxylate group in Glu257 and the backbone N-H of Ser 223, respectively. The carboxylate group of Glu257 expands the network by hydrogen bonding with the 1-hydroxyl group in the AMP portion of FAD. Lys258 complements the network with electrostatic and hydrogen bonding interactions with FAD that involve the side chain NH₃⁺ with the 2 pyrophosphate group and the terminal carboxylate with the 2'-ribityl hydroxyl, respectively.

Three important observations emerge from this analysis: (1) Residues in the AFVEK²⁵⁸ extension form an integral part of a complex network of interactions that associate the FAD and NADP⁺ cofactors with the enzyme. (2) The C'-terminal extension would have to undergo extensive conformational rearrangements to permit the formation of a “productive” complex with the nicotinamide and isoalloxazine rings stacked parallel and adjacent to one another. (3) Parallel stacking of these rings would also require large conformational changes in FAD, which would have to change from its folded conformation to perhaps the extended conformation characteristic of plastidic FNRs. This is unlikely because the folded conformation of FAD is stabilized by the network of interactions with NADP⁺ and the C'-terminal extension and because the absence of a sheet-loop-sheet motif in FPRs (see Figure 1) renders the enzyme incapable of stabilizing FAD in its extended conformation.

Consequently, in the context of current models for NADP⁺ binding to plastidic FNR enzymes, it seems unlikely that binding of the cofactor to *pa*-FPR would trigger the gross conformational rearrangement needed to allow parallel and adjacent placement of the nicotinamide and isoalloxazine rings in the *pa*-FPR-NADP complex. This in turn suggests that formation of a “productive” complex, in the sense of NADP⁺ binding to plastidic FNR, is not likely to occur with a frequency (μ s-ms) conducive to catalytical competence.

The Structure of *pa*-FPR Harbors a Pre-Formed NADP⁺ Binding Pocket

The binding of NADP⁺ brings about relatively minor structural changes to *pa*-FPR, as can be seen in the per-residue plot of ΔC_{α} (Figure 4-A), obtained by aligning the structures of *pa*-FPR and *pa*-FPR-NADP. The largest differences in C_{α} position, taken as $\Delta C_{\alpha} > 1.5$ times the average rmsd (0.47 Å) obtained from the alignment, are localized in the N-terminal of helix $\alpha 10$ (residues 221–225), the middle of the loop connecting $\alpha 10$ to $\beta 11$ (residues 242–244) and the carboxy terminal Lys 258. Among the affected amino acids, residues 221–225 and 258 are located in close proximity to the bound NADP⁺, whereas residues 242–244 are distant; the differences in C_{α} position seen for the latter are likely a consequence of the higher than average

B-factors exhibited by these residues. Figures 4-B and 4-C illustrate a portion of the surface of *pa*-FPR and *pa*-FPR-NADP, respectively. The side-by-side comparison reveals that the surface of *pa*-FPR has a pre-formed cavity where the NADP⁺ cofactor binds to form the *pa*-FPR-NADP complex with minimal perturbation of the *pa*-FPR structure.

It is well known that NADP⁺-dependent enzymes cannot substitute this cofactor for NAD⁺, a fact that is also evident in the negligible catalytic activity observed with *pa*-FPR when NADPH is replaced with NADH (6). Site directed mutagenesis studies indicated that stabilization of the 2'-P in NADP⁺ contributes significantly to the mechanism whereby NADP(H) dependent FNR enzymes discriminate against NAD(H) (25,26). In this context, it is interesting that in the crystal structure of *pa*-FPR a sulfate anion (from the crystallization solution) is nearly isostructural with the 2'-P group of NADP⁺ in the crystal structure of the *pa*-FPR-NADP complex. This is illustrated in Figure 4, where the sulfate in the structure of *pa*-FPR (Figure 4-D) exhibits interactions nearly identical those shown by the 2'-P group in the structure of the *pa*-FPR-NADP complex (Figure 4-E). These observations are in good agreement with the idea that the structure of *pa*-FPR harbors a pre-formed binding pocket, where residues involved in important contacts with the 2'P group of NADP⁺ require little or no rearrangement to accommodate the cofactor. Among these residues, R182 and R190 are conserved in bacterial subclass II reductases, Thr181 is conserved in bacterial subclass I enzymes and substituted for Ser in plant reductases (Ser223 in spinach FNR) and R182 is conserved in all enzymes with known sequence.

Assignment of Amide Backbone Resonances from *pa*-FPR

NMR spectroscopy studies were carried out to obtain complementary information in solution regarding the binding of NADP⁺ to *pa*-FPR. Before these investigations could begin, however, it was necessary to obtain sequential backbone resonance assignments. The relatively large molecular weight of the enzyme (29,518 Da) posed some challenges. These were overcome with the strategy described below. The ¹H-¹⁵N HSQC spectrum of *pa*-FPR acquired at 25 °C from a 1.2 mM solution of *pa*-FPR in 50 mM sodium phosphate buffer, pH 7.0 is shown in Figure 5-A. These conditions were chosen for the NMR spectroscopic studies because they completely eliminate the slow precipitation of the enzyme when its concentration exceeds 1.5 mM or when the samples are exposed to temperatures above 25 °C for 24 h or longer. The spectrum exhibits relatively well dispersed cross-peaks, despite the relatively large molecular weight of the enzyme. Conventional heteronuclear 2D and 3D NMR experiments (see Experimental) carried out with a sample of *pa*-FPR uniformly labeled with ¹³C and ¹⁵N did not yield enough information to permit full sequential assignments. This is mostly because many residues exhibited weak or absent beta carbon (C_β) correlations in TROSY-HNCACB and TROSY-CBCA(CO)NH experiments, which is attributed to efficient transverse relaxation brought about by the dipolar interactions between carbons and their attached protons (27). This problem was circumvented by preparing a sample of [U-²H, ¹³C, ¹⁵N]-*pa*-FPR, which was used to acquire TROSY-HNCACB and TROSY-CBCA(CO)NH experiments for subsequent use with the data obtained from the suite of experiments obtained with [U-¹³C, ¹⁵N]-*pa*-FPR. This approach allowed us to assign approximately 85% of the non-proline residues in the enzyme. With respect to [U-²H, ¹³C, ¹⁵N]-*pa*-FPR, it should be noted that although most of the exchangeable deuterons exchanged for protons during its purification, several residues are clearly protected from exchange because a number of cross-peaks displayed low-intensity or were absent when the HSQC spectrum of [U-²H, ¹³C, ¹⁵N]-*pa*-FPR was compared with that obtained from a sample of [U-¹⁵N, ¹³C]-*pa*-FPR. Deuterons protected from exchange under native conditions were exchanged by dissolving the triply labeled sample in a urea containing solution, followed by dialysis in the presence of FAD. This unfolding/refolding procedure resulted in complete replacement of exchangeable deuterons for protons, as indicated by the

fact that the TROSY-HSQC spectrum of the resultant enzyme is identical that obtained with doubly labeled *pa*-FPR.

Additional assignments were obtained by incorporating amino acid-selective ^{15}N labeling into *pa*-FPR. This strategy has been successfully utilized in our laboratories to complete the sequential backbone resonance assignments of a paramagnetic, highly helical heme oxygenase from *P. aeruginosa* (28). In the context of assigning the backbone resonances from *pa*-FPR, selective labeling was important in our strategy for two main reasons. (1) Nearly undetectable isotopic scrambling was observed with ^{15}N -Leu, ^{15}N -Phe, ^{15}N -Val and ^{15}N -Thr, as can be seen in the corresponding HSQC spectra (Figures S1-A to S1-D). Labeling with ^{15}N Gly scrambles the label to Ser (Figure S1-E). This type of scrambling, however was found to be useful because it aided in the identification of cross-peaks originating from Ser residues. The label in ^{15}N -Tyr also scrambles, albeit less selectively than the label in ^{15}N -Gly. Nevertheless, the information in the HSQC spectrum of ^{15}N -Tyr labeled *pa*-FPR (Figure S1-F) is valuable because most of the cross-peaks originating from ^{15}N -Tyr are significantly stronger than cross peaks originating from scrambled label. In contrast, the label in ^{15}N -Glu and ^{15}N -Asp is highly scrambled, as can be seen in the corresponding HSQC spectra of Figures S1-G and S1-H, respectively; these spectra were not very useful to the assignment process. Information obtained from selectively labeled samples was subsequently used in conjunction with the backbone connectivities derived from the suite of three-dimensional experiments described above in order to make the sequential assignments. This approach was essential to assign stretches in a sequence where spin systems of key residues within a segment could not be identified due to poor detection of C^{β} resonances. (2) The simplicity of HSQC spectra obtained from most amino acid-selective ^{15}N -*pa*-FPR samples allow identification of cross-peaks that can be easily overlooked in the spectrum of $[\text{U-}^{15}\text{N}]$ -labeled samples, because of overlap with other resonances or due to relative low intensity. For instance, in the HSQC spectrum of ^{15}N -Gly-*pa*-FPR the cross-peak in red corresponds to G205 (Figure S2). The same cross-peak is located in a crowded section of the spectrum obtained with $[\text{U-}^{15}\text{N}]$ -labeled enzyme and thus it had been overlooked. Its definitive identification in the spectrum of the ^{15}N -Gly-*pa*-FPR allowed its subsequent sequential assignment with the aid of the suite of three-dimensional experiments described above. In the end, the combined strategies allowed us to make 95% of backbone assignments in *pa*-FPR, not counting Pro; these assignments are summarized in Table S1.

Once assigned, the backbone chemical shifts were used to identify elements of secondary structure in solution by chemical shift indexing (CSI) (29). Results obtained from this process carried out with C_{α} chemical shifts have been plotted per residue in Figure 5-B, where they are compared with elements of secondary structure obtained from the crystal structure of *pa*-FPR using the program DSSP (<http://swift.cmbi.ru.nl/gv/dssp/>). It is apparent that secondary structure identified with the aid of NMR spectroscopic studies in solution is consistent with secondary structure obtained from the enzyme in crystal form. The most significant differences are in residues 191–197 ($\alpha 8$) and residues 199–204 ($\alpha 9$). The backbone resonances of residues in $\alpha 8$ were not assigned, most likely because the NH cross-peaks of these residues are very weak or unobservable in HSQC spectra, due to line broadening brought about by segmental dynamic behavior. Cross-peaks from residues 199–204, although observable, are significantly less intense than average, suggesting that these residues are also affected by dynamic conformational exchange. Hence, it is likely that this segment of the structure in solution is conformationally averaged between helical and disordered states; the fact that $\alpha 8$ and $\alpha 9$ are flanked by loops likely facilitates this segmental dynamic behavior. Interestingly, the crystal structure of the *pa*-FPR-NADP complex shows that $\alpha 8$ and $\alpha 9$ are in close proximity to the NADP^+ binding site, which suggests the possibility that local conformational plasticity prepares the enzyme to bind the NADP(H) cofactor.

Probing the Binding of NADP⁺ to *pa*-FPR in Solution by NMR Chemical Shift Perturbations

The binding of NADP⁺ to *pa*-FPR was studied by titrating NADP⁺ into a solution containing ¹⁵N-labeled *pa*-FPR, while monitoring induced chemical shift perturbations of amide ¹H and ¹⁵N resonances with the aid of ¹H-¹⁵N-HSQC spectra. The titration induced chemical shift perturbations larger than two times the average of the weighted chemical shift perturbation (0.12 ppm) in 22 cross-peaks, a characteristic that identifies the corresponding residues as potential sites of interaction with NADP⁺. The NADP⁺-dependent gradual shift of cross-peaks indicate that interconversion between NADP⁺-bound and free forms of the enzyme is fast relative to the NMR timescale (*i.e.* fast exchange). The titration also caused the disappearance of 18 cross-peaks, which is likely a consequence of exchange between bound and free forms at rates approximately equal to the chemical shift timescale (*i.e.* intermediate exchange). Cross-peaks exhibiting gradual chemical shift perturbations have been plotted per-residue (black in Figure 6-A), together with cross-peaks that disappear upon addition of NADP⁺ (red in Figure 6-A). The plot makes it evident that those residues whose chemical shifts exhibit gradual chemical shift perturbations (fast exchange) are clustered with residues whose chemical shifts disappear during the titration, which strongly suggests that line broadening of the latter is a consequence of binding interactions that trigger dynamic events taking place in the intermediate exchange regime. The NADP⁺-dependent chemical shift perturbation of cross-peaks in fast exchange has been plotted for several representative amino acids (V144, W146 and V147) in Figure S3-A and the curve fitted to a model where one molecule of *pa*-FPR binds one molecule of NADP⁺. This analysis reveals an average dissociation constant (K_d) of 24 μ M, a value similar that reported for the binding of NADP⁺ to spinach FNR (14 μ M) at lower ionic strength (30).

Residues whose N-H cross-peaks exhibit weighted chemical shift perturbations larger than 0.08 ppm upon titrating *pa*-FPR with NADP⁺ are highlighted in green on the X-ray crystal structure of the *pa*-FPR-NADP complex (Figure 6-C), whereas residues whose N-H cross-peaks disappear are highlighted in red. It is reassuring that the chemical shifts of amide cross-peaks corresponding to residues identified in the crystal structure as being in close proximity to NADP⁺ are perturbed by the presence of NADP⁺. Amongst these, cross-peaks from residues interacting with the 2'-P group of NADP⁺, Thr181, Arg182 and Arg190 (see Figure 3), are broadened and disappear due to exchange in the intermediate regime, whereas the cross-peak originating from Glu257, which interacts with the amide NH₂ group of the nicotinamide ring exhibits perturbations in the fast exchange regime. Cross peaks for Arg145 and Ser223, which interact with the pyrophosphate group P1, and with both the nicotinamide amide and the 2'P groups of NADP⁺, respectively, have not been assigned. A comparison of the X-ray crystal structures of *pa*-FPR and *pa*-FPR-NADP has been made in Figures 4-B and 4-C, which shows that the structure of *pa*-FPR has a pre-formed "NADP⁺ binding pocket" where the cofactor binds with minimal perturbations on the structure of the enzyme. In Figure 6-C, the cofactors have been rendered in sticks to illustrate the fact that residues comprising the "internal walls" of the "NADP⁺ binding pocket" are highlighted in red and green. This observation indicates that the surface of interaction in the structure of NADP⁺ includes the "internal walls" of the "NADP⁺ binding pocket", and demonstrates that the chemical shift perturbations and line broadening effects brought about by the binding of NADP⁺ in solution delineate a binding surface highly consistent with that observed in the crystal structure. Hence, observations made with the enzyme in solution also indicate that the structure of *pa*-FPR harbors a pre-formed "NADP⁺ binding pocket".

Current models of NADP(H) binding to plastidic FNRs propose that parallel stacking of the nicotinamide ring onto the isoalloxazine ring to form a "productive" complex for direct hydride transfer requires displacement of the side chain from the terminal Tyr. Equilibrium binding studies conducted with spinach FNR revealed that its binding affinity for NADP⁺ is

approximately seven times lower than its affinity for adenosine 2',5'-diphosphate (ADP) (30), which lacks the nicotinamide nucleotide moiety. These observations have been interpreted in the context of the binding model to support the idea that NADP(H) binding to plastidic FNRs is a two-step process, with the first step involving strong interactions between the 2'-adenosyl phosphate and FNR, and the second step requiring displacement of the terminal Tyr to allow the nicotinamide ring to stack parallel to the isoalloxazine ring of FAD. In this model, the second step, which is thought to be energetically costly, has been invoked to explain the higher affinity of FNR for ADP relative to NADP⁺ (17,31). It was therefore of interest to examine the binding of ADP to *pa*-FPR and compare the results with those described above for the binding of NADP⁺. Hence, ADP was titrated into a solution containing ¹⁵N-labeled *pa*-FPR, while monitoring induced chemical shift perturbations in ¹H-¹⁵N-HSQC spectra. Remarkably, titration with ADP revealed a pattern of perturbed residues (Figure 6-B) nearly identical to the pattern obtained upon binding of NADP⁺ to *pa*-FPR (Figure 6-A). This fact is also evident in the corresponding color coded representation obtained by mapping residues whose cross-peaks exhibit chemical shift perturbations (green) and line broadening effects (red) on the structure of *pa*-FPR-NADP (Figure 6-D). Chemical shift perturbations induced by addition of ADP to *pa*-FPR for several representative amino acids (V144, W146 and V147) have been plotted and fitted to a model with stoichiometry 1:1 (Figure S3-B). This process reveals an average K_d of 32 μM, a value that is slightly larger than that measured for the *pa*-FPR-NADP complex (see above). The similarity in the magnitudes of K_d obtained for the binding of NADP⁺ and the competitive inhibitor ADP indicates that stabilization of the *pa*-FPR-NADP complex is derived mainly from interactions between the polypeptide and the adenosine 2', 5'-diphosphate moiety in NADP⁺. In contrast to observations made with spinach FNR, however, the binding affinity of *pa*-FPR for NADP⁺ is slightly larger than its affinity for ADP, which indicates that the nicotinamide nucleotide moiety does not undergo destabilizing interactions with the enzyme, as is thought to be the case in the binding of NADP⁺ to plastidic FNRs. It is therefore likely that NADP⁺ binding to *pa*-FPR occurs in one step, rather than two, as is thought to be the case when it binds to FNRs.

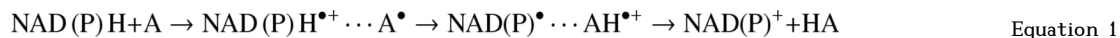
The C'-terminal sequence is unlikely to experience large conformational disorder

As pointed out above, the X-ray crystal structure of *pa*-FPR revealed a network of interactions involving the C'-terminal extension and the two cofactors, strongly suggesting that the C'-terminal sequence of *pa*-FPR is not likely to be displaced readily in order to allow parallel stacking of the nicotinamide and isoalloxazine rings. To examine whether the C'-terminal tail is undergoing conformational fluctuations in solution we looked for signs of dynamic motions manifested in the characteristics of HSQC cross-peaks. Peaks significantly affected by slow conformational exchange (μs-ms) typically show decreased intensity and/or larger line-widths than those originating from regions of a protein unaffected by such motions, provided the inter-converting species in equilibrium are sufficiently populated (32,33). In this analysis, we expected that residues located near the nicotinamide and isoalloxazine rings would be most significantly affected by conformational exchange, and consequently display enhanced line widths and/or decreased intensity relative to the average for all other peaks in the spectrum. This notion was probed in solution by acquiring ¹H-¹⁵N-HSQC spectra of *pa*-FPR, *pa*-FPR-NADP and *pa*-FPR-ADP at different temperatures (35 °C, 25 °C and 15 °C) and at 600 MHz ¹H frequency. Cross-peaks corresponding to the AFVEK²⁵⁸ sequence exhibit ¹H linewidths and cross-peak intensities that are very similar to the average ¹H linewidths and average cross-peak intensity at each of the temperatures in all spectra, implying that alternative conformations are not significantly populated in the range of temperature explored, thus suggesting that the C'-terminal extension is unlikely to undergo significant conformational changes, in the presence or in the absence of NADP⁺. It is important to note that the data at hand cannot completely rule out the presence of a dynamic equilibrium between a very low population of molecules, where the cofactors attain a "productive conformation", and a bulk

population where the conformation of FAD and NADP⁺ is very similar to that in the crystal structure, which dominates the HSQC spectrum. If this small population is indeed present, it may be possible to study it with the aid of detailed dynamic studies, including analysis of R₂ relaxation dispersion data (32,34). It is important to consider, however, that the population with a “productive conformation” is low in the plastidic FNRs (~ 10%) (17), where only the side chain of the terminal Tyr has to move to allow the nicotinamide ring of NADP⁺ to enter the FAD-isoalloxazine environment. In comparison, the structure of the *pa*-FPR-NADP complex indicates that for the nicotinamide ring to enter the isoalloxazine environment, a much larger conformational rearrangement is necessary, which involves the AFVEK²⁵⁸ terminal extension. Moreover, it is also important to consider that the conformation of FAD in *pa*-FPR is bent and therefore distinct from the extended FAD conformation in plastidic FNRs (see Figure 1). The bent conformation of FAD in bacterial FPR enzymes places the adenine ring between the isoalloxazine and nicotinamide rings (see Figure 3). Consequently, for the nicotinamide ring to enter the isoalloxazine ring environment in bacterial FPRs, the FAD has to undergo a large conformational change, which very likely would expose a large portion of the cofactor to the aqueous environment, thus making it prone to be released from the enzyme. It is also conceivable that binding of NADPH instead of NADP⁺ promotes the large conformational changes that would be needed to form a “productive” complex in FPRs. This scenario, however, is also unlikely because the conformational changes necessary would still involve the large amplitude motions of the C'-terminal sequence and of the FAD cofactor discussed above. Hence, together, these considerations strongly suggest that the large conformational changes that would have to take place on FPR to allow parallel and adjacent placement of the nicotinamide and isoalloxazine rings for direct hydride transfer are unlikely. Nevertheless, additional experimentation is necessary to continue to probe these ideas.

Potential Implications to the Mechanism of NADPH Oxidation by FPRs

The above-described observations suggest that conformational reorganization of the C'-terminal peptide and of the NADP⁺ and FAD cofactors to allow formation of a “productive” complex for direct hydride transfer is unlikely to take place in the *pa*-FPR-NADP complex. In this context, it is important to consider that extensive fundamental investigations of the mechanism of NAD(P)H oxidation have demonstrated that hydride transfer can also occur in a stepwise manner by sequential electron-proton-electron transfer (35-44) (Equation 1). These investigations documented the formation of radical cations and radicals of



NAD(P)H and its analogues, which have been characterized with the aid of electronic absorption and EPR spectroscopic methods. The formation and detection of these reactive species indicated that the oxidation of NAD(P)H and its analogues can occur stepwise via electron-proton-electron transfer of hydride, if the acceptor is also capable of undergoing a stepwise two electron reduction. This point has been recently underscored with the EPR and electronic absorption spectroscopic detection of a radical cation of an NADH analogue in the thermal two-electron reduction of a quinone (35). Moreover, it has also been demonstrated that in the absence of H₂O₂, the oxidation of NADH by native horseradish peroxidase (HRP) begins with single-electron transfer from NADH to ferric HRP to form the NADH^{•+} radical cation and ferrous peroxidase (39). A similar stepwise oxidation of NADPH is thought to be operative in the rescue of inactive catalase (45). Hence, under appropriate circumstances the oxidation of NAD(P)H by sequential electron-proton-electron transfer of hydride is a viable alternative mechanistic path to the well-known direct mechanism involving synchronous transfer of a proton and two electrons.

It has also been established that long-range (up to 30 Å) electron transfer through proteins occurs via tunneling pathways, which involve dominant bonding and nonbonding interactions coupling donor and acceptor. Coupling through covalent and hydrogen bonds is stronger than coupling through van der Waals gaps (46-48), and these differences in the details of specific paths involved in distinct systems account for the dependence of electron transfer rates on the particular aspects of the protein structure that mediate coupling of donor and acceptor (48). In this frame it is interesting that the structure of the *pa*-FPR-NADP complex places C4 of the nicotinamide ring 14.5 Å away from N5 of the isoalloxazine ring. Further inspection of the structure suggests a “tunneling pathway” connecting the nicotinamide ring in NADP(H) with the isoalloxazine ring in FAD. This putative path (Figure 7-A) can be thought to start with the T-stacking of the nicotinamide and Phe255 rings, continue along Phe255 into Ala254 across the peptide bond and finally communicate with the isoalloxazine ring via the Ala254 carbonyl oxygen, which is 2.93 Å from the N10 and 3.93 Å from the N5 atom in the isoalloxazine ring. In this putative mechanism, electron tunneling from the nicotinamide to the isoalloxazine ring would form an NADPH^{•+} radical cation analogous that shown in Equation 1. Radical cations of NADH model compounds are known to be significantly more acidic than their neutral precursors (42), thus, the NADPH^{•+} radical cation formed upon tunneling of one electron would be expected to lose a proton thereby forming an NADP[•] radical, as shown in Equation 1. Tunneling of a second electron from the latter would form the closed shell NADP⁺.

Accordingly, the electron acceptor, FAD, can be reduced in two sequential one-electron and one proton transfer reactions (49,50). In the context of a stepwise, electron-proton-electron, hydride transfer, it is also interesting to note a network of structural water molecules in the structure of the *pa*-FPR-NADP complex, which may facilitate proton translocation from NADPH to FAD (Figure 7-B). In the same frame, it is also interesting to consider that amino acid alignment of bacterial subclass I FPR enzymes (Figure 7-C) shows that the AFVEK²⁵⁸ extension of *pa*-FPR is present in all bacterial subclass I FPR enzymes of known sequence (AFVxx). Furthermore, it is noteworthy that residues A²⁵⁴ and F²⁵⁵ in this motif, which we implicate in the putative path of electron transfer (Figure 7-A), are conserved.

It is important to emphasize that one-electron reduction of NAD(P)⁺ analogues does not result in an overall hydride ion addition in the same manner in which one-electron oxidation of NAD(P)H triggers a multistep hydride ion release (38). Hence, the proposed mechanism of NADPH oxidation by FPRs is consistent with the fact that these enzymes function by exclusively oxidizing the cofactor, unlike their plastidic counterparts, which function in the “normal” sense by reducing NADP⁺ via hydride transfer from FADH₂ or in the “inverse” sense by oxidizing NADPH. It is therefore possible that the need to reduce NADP⁺ has placed evolutive pressure on the structure of plastidic FNRs to allow parallel placement of the nicotinamide and isoalloxazine rings for efficient hydride transfer and reduction of NADP⁺ in order to support the high electron flow needed in the photosynthetic process of CO₂ fixation (5). In comparison, the function of FPR enzymes, which is solely the oxidation of NADPH, was acquired with minor modifications of the C'-terminal domain, which make the direct transfer of hydride (NADP⁺ reduction) unlikely but a multistep hydride transfer (NADPH oxidation) operative. These ideas, which stem from the X-ray crystallographic and NMR spectroscopic observations of the *pa*-FPR-NADP complex, have to be tested experimentally. Their discussion in this report is aimed at providing a frame of ideas consistent with experimental observations and to stimulate future experimentation directed at elucidating the mechanism of NADPH oxidation by FPR enzymes.

Supplementary Material

Refer to Web version on PubMed Central for supplementary material.

REFERENCES

1. Arakaki AK, Ceccarelli EA, Carrillo N. Plant-Type Ferredoxin NADP⁺ Reductases: A Basal Structural Framework and a Multiplicity of Functions. *FASEB J* 1997;11:133–140. [PubMed: 9039955]
2. Shin M, Arnon DI. Enzymic Mechanisms of Pyridine Nucleotide Reduction in Chloroplasts. *J Biol Chem* 1965;240:1405–1411. [PubMed: 14284756]
3. Liochev SI, Hausladen A, Beyer WFJ, Fridovich I. NADPH:Ferredoxin Oxidoreductase Acts as a Paraquat Diaphorase and is a Member of the *soxRS* Regulon. *Proc. Natl. Acad. Sci. USA* 1994;91:1328–1331. [PubMed: 8108411]
4. Yannone SM, Burgess BK. The Seven-Iron FdI from *Azotobacter vinelandii* Regulates the Expression of NADPH:Ferredoxin Reductase via an Oxidative Stress Response. *J. Biol. Inorg. Chem* 1998;3:253–258.
5. Bittel C, Tabares LC, Armesto M, Carrillo N, Cortez N. The oxidant-Responsive Diaphorase of *Rhodobacter capsulatus* is a Ferredoxin (flavodoxin)-NADP(H) Reductase. *FEBS Lett* 2003;553:408–412. [PubMed: 14572660]
6. Wang A, Zeng Y, Han H, Weeratunga S, Morgan BN, Moënn-Loccoz P, Schönbrunn E, Rivera M. Biochemical and Structural Characterization of *Pseudomonas aeruginosa* Bfd and FPR: Ferredoxin NADP⁺ Reductase and Not Ferredoxin is the Redox Partner of Heme Oxygenase under Iron-Starvation Conditions. *Biochemistry* 2007;46:12198–12211. [PubMed: 17915950]
7. Prasad GS, Kresge N, Muhlberg AB, Shaw A, Jung YS, Burgess BK, Stout CD. The Crystal Structure of NADPH:Ferredoxin Reductase from *Azotobacter vinelandii*. *Protein Sci* 1998;7:2541–2549. [PubMed: 9865948]
8. Nogués I, Pérez-Dorado I, Frago S, Bittel C, Mayhew SG, Gómez-Moreno C, Hermoso JA, Medina M, Cortez N, Carrillo N. The Ferredoxin-NADP(H) Reductase from *Rhodobacter capsulatus*: Molecular Structure and Catalytic Mechanism. *Biochemistry* 2005;44:11730–11740. [PubMed: 16128574]
9. Ingelman M, Bianchi V, Eklund H. The Three-Dimensional Structure of Flavodoxin Reductase from *Escherichia coli* at 1.7 Å Resolution. *J. Mol. Biol* 1997;268:147–157. [PubMed: 9149148]
10. Ceccarelli EA, Arakaki AK, Cortez N, Carrillo N. Functional Plasticity and Catalytic Efficiency in Plant and Bacterial Ferredoxin-(NADP(H) Reductases. *Biochim. Biophys. Acta* 2004;1698:155–165. [PubMed: 15134648]
11. Karplus PA, Daniels MJ, Herriott DJR. Atomic Structure of Ferredoxin-NADP⁺ Reductase: Prototype for a Structurally Novel Flavoenzyme Family. *Science* 1991;251:60–66. [PubMed: 1986412]
12. Bruns CM, Karplus PA. Refined Crystal Structure of Spinach Ferredoxin Reductase at 1.7 Å Resolution: Oxidized Reduced and 2'-phospho-5'AMP Bound States. *J. Mol. Biol* 1995;247:125–145. [PubMed: 7897656]
13. Hermoso JA, Mayoral T, Faro M, Gómez-Moreno C, Sanz-Aparicio J, Medina M. Mechanism of Coenzyme Recognition and Binding Revealed by Crystal Structure Analysis of Ferredoxin-NADP⁺ Reductase Complexed with NADP⁺. *J. Mol. Biol* 2002;319:1133–1142. [PubMed: 12079352]
14. Serre L, Vellieux FMD, Medina M, Gómez-Moreno C, Fontecilla-Camps JC, Frey M. X-ray Structure of the Ferredoxin:NADP⁺ Reductase from the Cyanobacterium *Anabaena* PCC7119 at 1.8 Å Resolution, and Crystallographic studies of NADP⁺ Binding at 2.25 Å Resolution. *J. Mol. Biol* 1996;263:20–39. [PubMed: 8890910]
15. Pai EF, Karplus PA, Schulz GE. Crystallographic Analysis of the Binding of NADPH, NADPH Fragments, and NADPH Analogues to Glutathione Reductase. *Biochemistry* 1988;27:4465–4474. [PubMed: 2844232]
16. Karplus PA, Schulz GE. Substrate Binding and Catalysis by Glutathione Reductase as Derived from Refined Enzyme: Substrate Crystal Structures at 2 Å Resolution. *J. Mol. Biol* 1989;210:163–180. [PubMed: 2585516]
17. Deng Z, Aliverti A, Zanetti G, Arakaki AK, Ottado J, Orellano EG, Calcaterra NB, Ceccarelli EA, Carrillo N, Karplus PA. A Productive NADP⁺ Binding Mode of Ferredoxin-NADP⁺ Reductase Revealed by Protein Engineering and Crystallographic Studies. *Nature Struct. Biol* 1999;6:847–853. [PubMed: 10467097]

18. Morgan WD, Kragt A, Feeney J. Expression of deuterium-isotope-labelled protein in the yeast *Pichia pastoris* for NMR studies. *Journal of Biomolecular NMR* 2000;17:337–347. [PubMed: 11014598]
19. Cheng H, Westler WM, Xia B, Oh B-H, Markley JL. Protein expression, selective isotopic labeling, and analysis of hyperfine-shifted NMR signals of *Anabaena* 7120 vegetative [2Fe-2S]ferredoxin. *Archives of Biochemistry and Biophysics* 1995;316:619–634. [PubMed: 7840674]
20. Rodriguez JC, Wilks A, Rivera M. Backbone NMR Assignments and H/D Exchange Studies on the Ferric Azide- and Cyanide-Inhibited Forms of *Pseudomonas aeruginosa* Heme Oxygenase. *Biochemistry* 2006;45:4578–4592. [PubMed: 16584193]
21. Wishart DS, Bigam CG, Yao J, Abildgaard F, Dyson HJ, Oldfield E, Markley JL, Sykes BD. ^1H , ^{13}C and ^{15}N Chemical Shift Referencing in Biomolecular NMR. *J. Biomol. NMR* 1995;6:135–140. [PubMed: 8589602]
22. Kabsch W. Automatic Processing of Rotation Diffraction Data from Crystals of Initially Unknown Symmetry and Cell Constraints. *J. Appl. Crystallogr* 1993;26:795–800.
23. Brunger AT, Adams PD, Clore GM, DeLano WL, Gros P, Grosse-Kunstleve RW, Jiang JS, Kuszewski J, Nilges M, Pannu NS, Read RJ, Rice LM, Simonson T, Warren GL. Crystallography & NMR System: A New Software Suite for Macromolecular Structure Determination. *Acta Crystallogr* 1998;D54:905–921.
24. Jones TA, Zhou JY. Improved Methods for Binding Protein Models in Electron Density Maps and the Location of Errors in These Models. *Acta Crystallogr Section A: Foundations of Crystallography* 1991;A47:110–119.
25. Medina M, Luquita A, Tejero J, Hermoso J, Mayoral T, Sanz-Aparicio J, Grever K, Gómez-Moreno C. Probing the Determinants of Coenzyme Specificity in Ferredoxin NADP⁺ Reductase by Site-Directed Mutagenesis. *J. Biol. Chem* 2001;276:11902–11912. [PubMed: 11152461]
26. Medina M, Gómez-Moreno C. Interaction of Ferredoxin-NADP⁺ Reductase with its Substrates: Optimal Interaction for Efficient Electron Transfer. *Photophys. Res* 2004;79:113–131.
27. Permi P, Annala A. Coherence Transfer in Proteins. *Prog. Nucl. Mag. Res. Sp* 2004;44:97–137.
28. Rodríguez JC, Zeng Y, Wilks A, Rivera M. The Hydrogen-Bonding Network in Heme Oxygenase Also Functions as a Modulator of Enzyme Dynamics: Chaotic Motions upon Disrupting the H-Bond Network in Heme Oxygenase from *Pseudomonas aeruginosa*. *J. Am. Chem. Soc* 2007;129:11730–11742. [PubMed: 17764179]
29. Wishart DS, Sykes BD. The ^{13}C Chemical-Shift Index: A Simple Method for the Identification of Protein Secondary Structure Using ^{13}C Chemical Shift Data. *J. Biomol. NMR* 1994;4:171–180. [PubMed: 8019132]
30. Batie CJ, Kamin H. Association of Ferredoxin-NADP⁺ Reductase with NADP(H). Specificity and Oxidation-Reduction Properties. *J Biol Chem* 1986;261:11214–11223. [PubMed: 3755438]
31. Carrillo N, Ceccarelli EA. Open Questions in Ferredoxin-NADP⁺ Reductase Catalytic Mechanism. *Eur. J. Biochem* 2003;270:1900–1915. [PubMed: 12709048]
32. Millet O, Loria JP, Kroenke CD, Pons M, Palmer AG. The Static Magnetic Field Dependence of Chemical Exchange Line Broadening Defines the NMR Chemical Shift Time Scale. *J. Am. Chem. Soc* 2000;122:2867–2877.
33. Zhang O, Forman-Kay JD. NMR Studies of Unfolded States of an SH3 Domain in Aqueous Solution and Denaturing Conditions. *Biochemistry* 1997;36:3959–3970. [PubMed: 9092826]
34. Boehr DD, McElheny D, Dyson HJ, Wright PE. The Dynamic Energy Landscape of Dihydrofolate Reductase Catalysis. *Science* 2006;313:1638–1642. [PubMed: 16973882]
35. Yuasa J, Yamada S, Fukuzumi S. Detection of a Radical Cation of an NADH Analogue in Two-Electron Reduction of a Protonated *p*-Quinone Derivative by an NADH Analogue. *Agew. Chem. Int. Ed* 2008;47:1068–1071.
36. Fukuzumi S, Inada O, Suenobu T. Direct Detection of Radical Cations of NADH Analogues. *J. Am. Chem. Soc* 2002;124:14538–14539. [PubMed: 12465955]
37. Fukuzumi S, Inada O, Suenobu T. Mechanisms of Electron-Transfer Oxidation of NADH Analogues and Chemiluminescence. Detection of the Keto and Enol Radical Cations. *J. Am. Chem. Soc* 2003;125:4808–4816. [PubMed: 12696900]
38. Gębicki J, Marcinek A, Zielonka J. Transient Species in the Stepwise Interconversion of NADH and NAD⁺ Acc. Chem. Res 2004;37:379–386. [PubMed: 15196047]

39. Afanasyeva MS, Taraban MB, Purtov PA, Lashina TV, Grissom CB. Magnetic Spin Effects in Enzymatic Reactions: Radical Oxidation of NADH by Horseradish Peroxidase. *J. Am. Chem. Soc* 2006;128:8651–8658. [PubMed: 16802831]
40. Yuasa J, Fukuzumi S. Mechanistic Borderline Between One-Step Hydrogen Transfer and Sequential Transfers of Electron and Proton in Reactions of NADH Analogues with Triplet Excited States of Tetrazines and Ru(bpy)²⁺. *J. Am. Chem. Soc* 2006;128:14281–14292. [PubMed: 17076501]
41. Fukuzumi S, Ohkubo K, Tokuda Y, Suenobu T. Hydride Transfer from 9-Substituted 10-Methyl-9,10-dihydroacridines to Hydride Acceptors via Charge-Transfer Complexes and Sequential Electron-Proton-Electron Transfer. A negative Temperature Dependence. *J. Am. Chem. Soc* 2000;122:4286–4294.
42. Anne A, Hapiot P, Moiroux J, Neta P, Savéant JM. Dynamics of Proton Transfer from Cation Radicals. Kinetic and Thermodynamic Acidities of Cation Radicals of NADH Analogues. *J. Am. Chem. Soc* 1992;114:4694–4701.
43. Zielonka J, Marcinek A, Huben K, Gębicki J. Direct Observation of NADH Radical Cation Generated in Reactions with One-Electron Oxidants. *J. Phys. Chem. A* 2003;107:9860–9864.
44. Marcinek A, Adamus J, Huben K, Gębicki J, Bartczak TJ, Bednarek P, Bally T. Hydrogen-Transferred Radical Cations of NADH Model Compounds. 1. Spontaneous Tautomerization. *J. Am. Chem. Soc* 2000;122:437–443.
45. Almarsson O, Sinha A, Gopinath E, Bruice TC. Mechanism of One-Electron Oxidation of NAD(P)H and Function of NADPH Bound to Catalase. *J. Am. Chem. Soc* 1993;115:7093–7102.
46. Beratan DN, Betts JN, Onuchic JN. Protein Electron Transfer Rates Set by the Bridging Secondary and Tertiary Structure. *Science* 1991;252:1285–1288. [PubMed: 1656523]
47. Beratan DN, Onuchic JN, Betts JN, Bowler BE, Gray HB. Electron-Tunneling Pathways in Ruthenated Proteins. *J. Am. Chem. Soc* 1990;112:7915–7921.
48. Gray HB, Winkler JR. Long-Range Electron Transfer. *Proc. Natl. Acad. Sci. USA* 2005;102:3534–3539. [PubMed: 15738403]
49. Bhattacharyya S, Stankovich MT, Truhlar DG, Gao J. Combined Quantum Mechanical and Molecular Mechanical Simulations of One- and Two-Electron Reduction Potentials of Flavin Cofactor in Water, Medium-Chain Acyl-CoA Dehydrogenase, and Cholesterol Oxidase. *J. Phys. Chem* 2007;111:5279–5742.
50. Ghisla S, Massey V. Mechanisms of Flavoprotein-Catalyzed Reactions. *Eur. J. Biochem* 1989;181:1–17. [PubMed: 2653819]

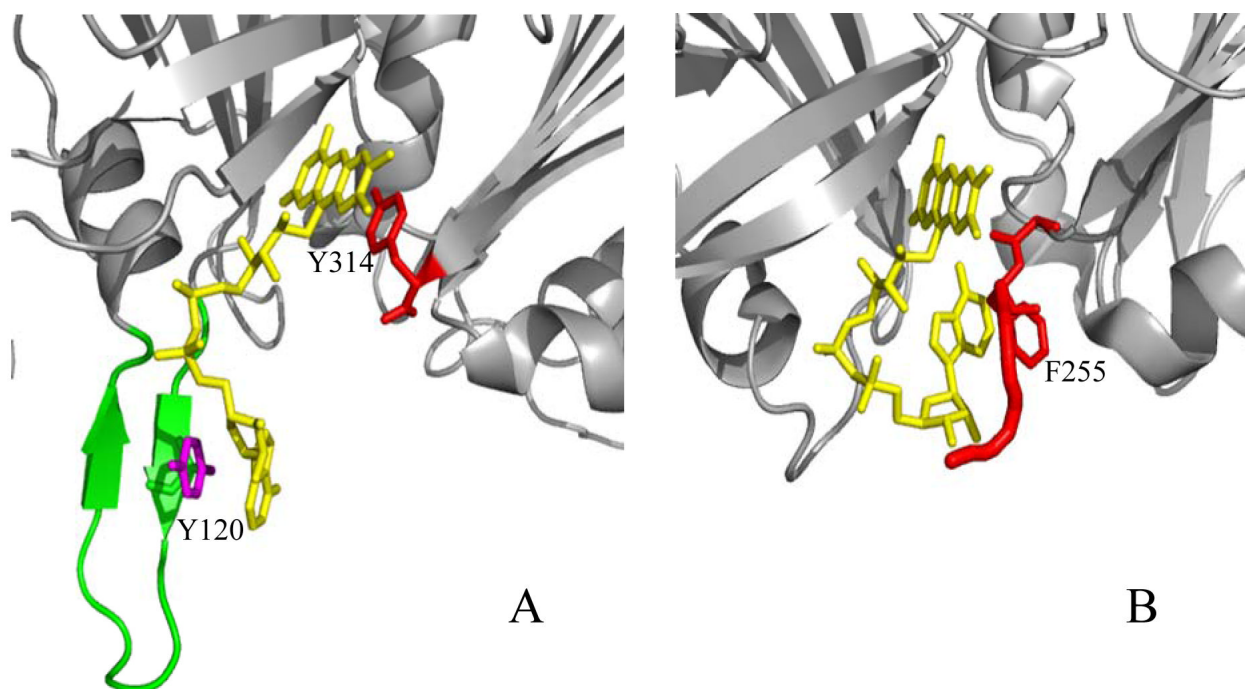


Figure 1.

(A) The fold of plastidic FNRs exhibits a conserved sheet-loop sheet motif (green) that contributes to stabilizing the extended FAD (yellow) conformation characteristic of these enzymes. (B) The fold of bacterial FPRs is devoid of the sheet-loop-sheet motif and exhibits a characteristically bent FAD conformation and a C'-terminal extension (red).

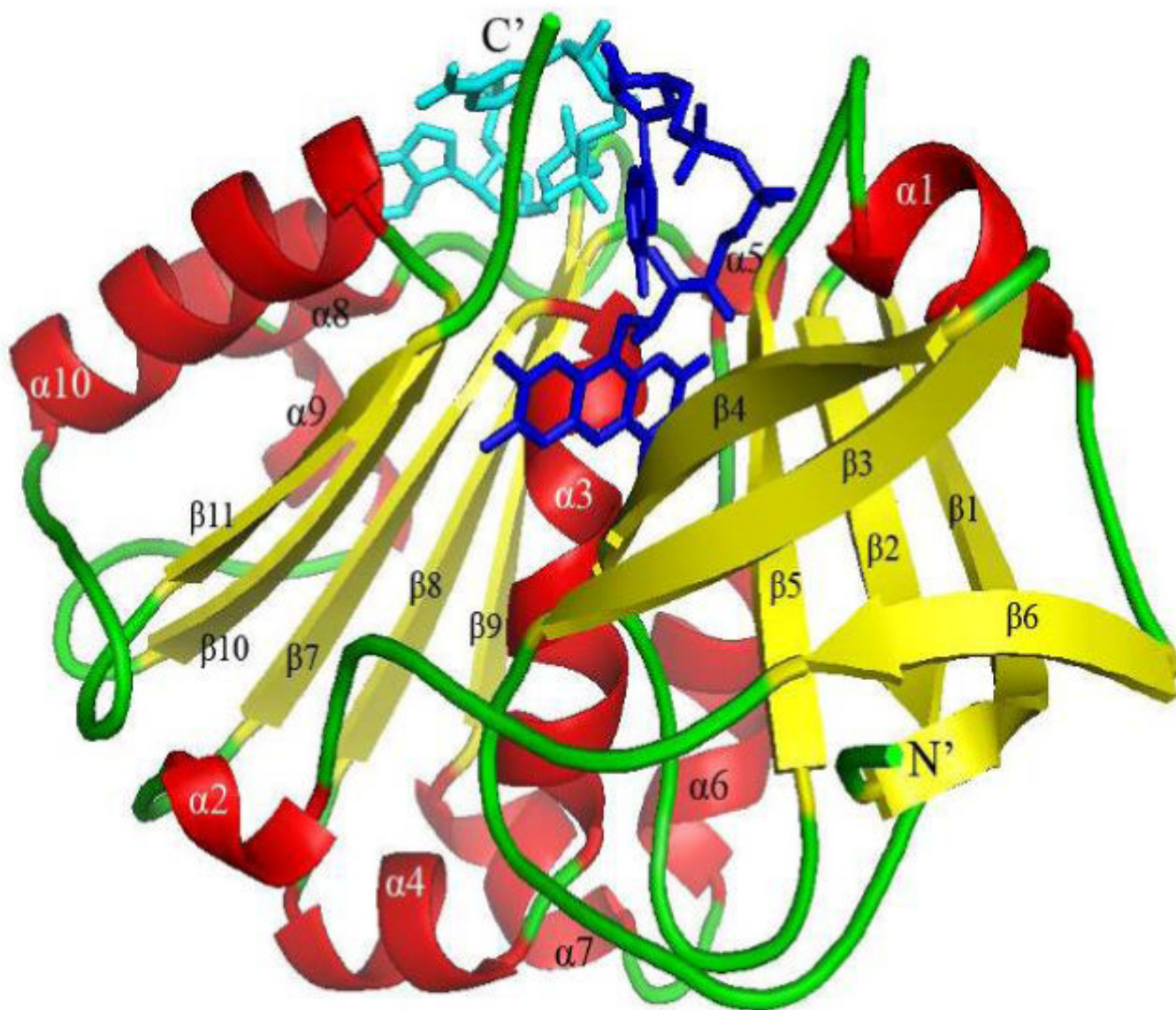


Figure 2. View of the structure of the *pa*-FRP bound to NADP⁺. FAD is shown in blue, NADP⁺ in cyan, α -helices in red, β -sheets in yellow and loops in green.

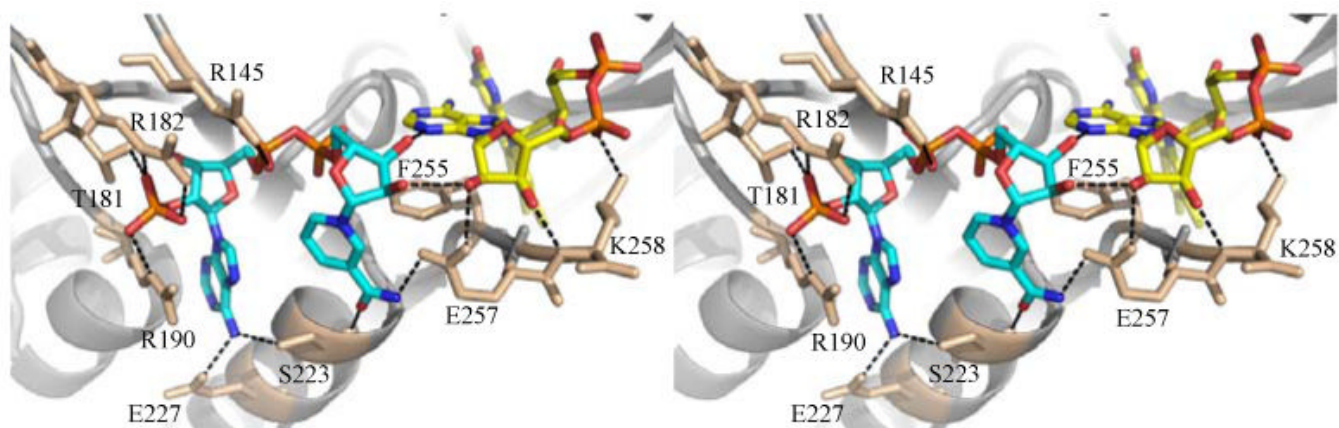


Figure 3.

Stereoview of a portion of the structure of *pa*-FPR-NADP highlighting the network of stabilizing interactions between the C'-terminal extension (AFVEK²⁵⁸) and the cofactors. FAD is shown in yellow and NADP⁺ in cyan, with their N, O and P atoms in blue, red and orange, respectively.

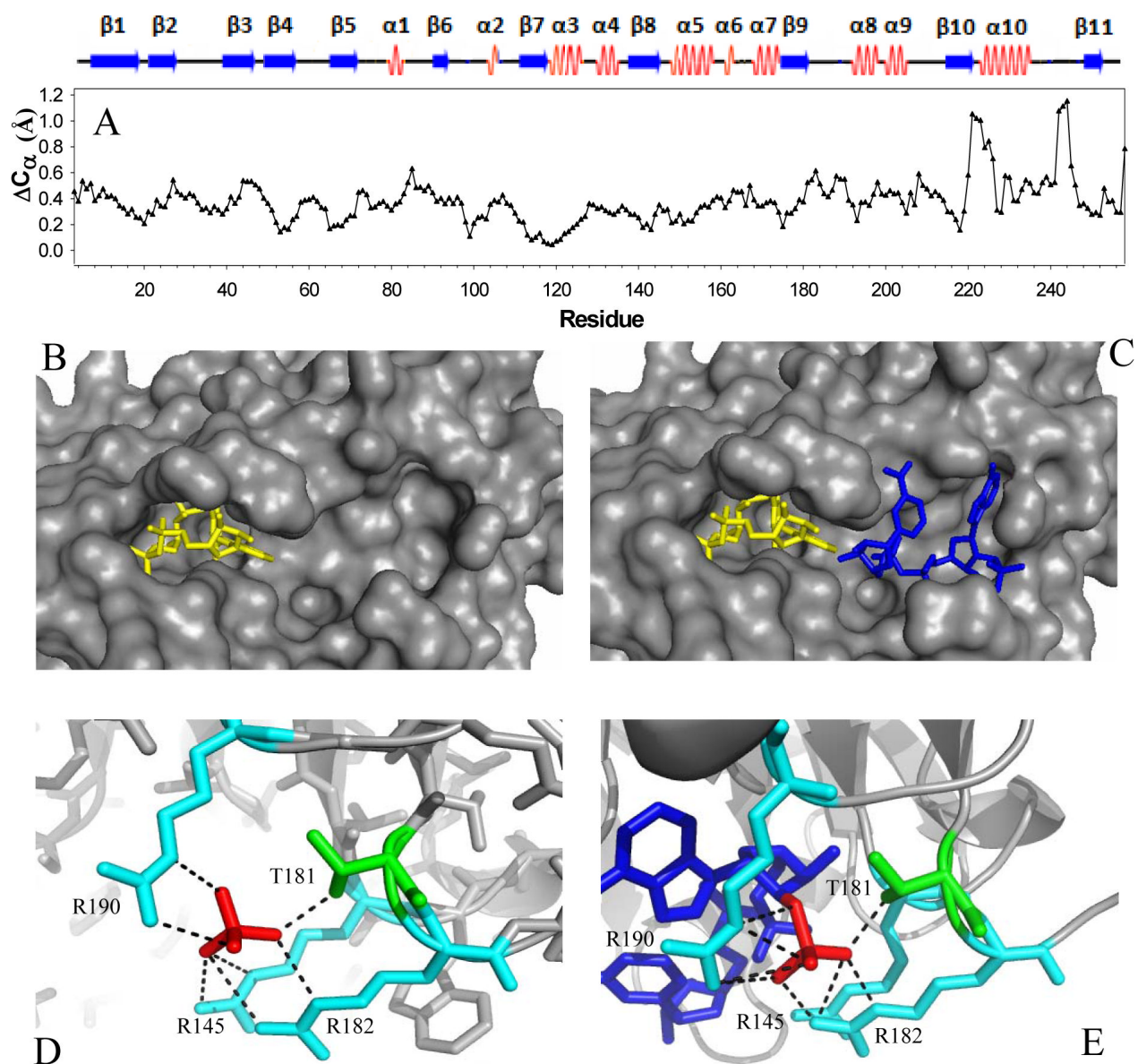


Figure 4.

(A) Per residue plot of the difference in the position of alpha carbons (ΔC_{α}) obtained upon aligning the structures of *pa*-FPR and that of its NADP⁺ complex. The average RMSD is 0.47 Å. (B) Close-up view of the empty “NADP-binding pocket” on the surface of *pa*-FPR; the FAD is rendered in yellow sticks. (C) Equivalent view, obtained from the structure of the *pa*-FPR-NADP complex, highlighting NADP⁺ (blue sticks) lodged in its binding pocket. (D) The structure of *pa*-FPR displays a sulfate ion (red) from the crystallization buffer that occupies the position of the 2'-phosphate group in the *pa*-FPR-NADP complex (E). Note that the interactions exhibited by the phosphate and sulfate ions are nearly identical.

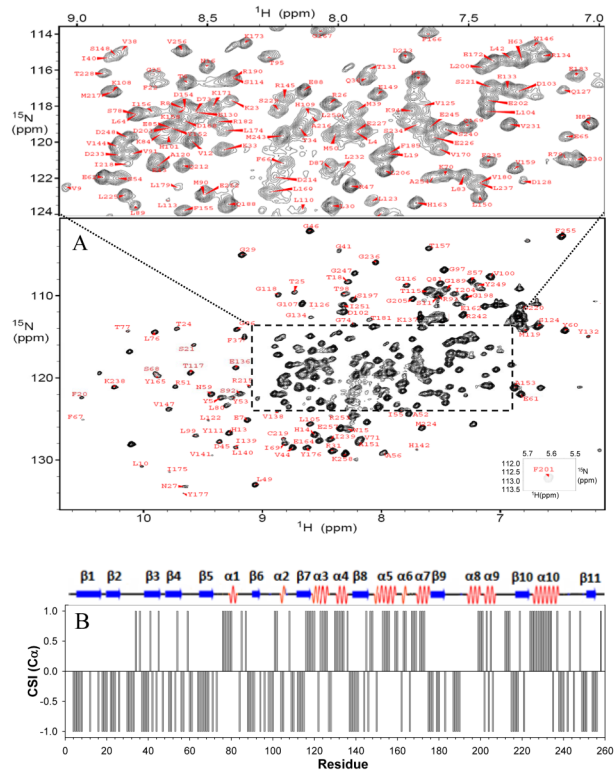


Figure 5.

(A) ^1H - ^{15}N HSQC of 1.5 mM $[\text{U-}^{13}\text{C}, ^{15}\text{N}]$ -*pa*-FPR in 50 mM sodium phosphate, pH 7.0, and 6% D_2O , obtained at 25 °C using a Bruker Avance800 NMR spectrometer. Complex points, 256 (^1H) x 2048 (^{15}N); spectral width, 14.4 kHz (^1H) and 3.3 kHz (^{15}N); 4 scans per increment, recycle delay 0.8s. (B) Secondary structure in *pa*-FPR inferred from chemical shift indexing (C_α), which can be compared to secondary structure inferred from the X-ray crystal structure (top).

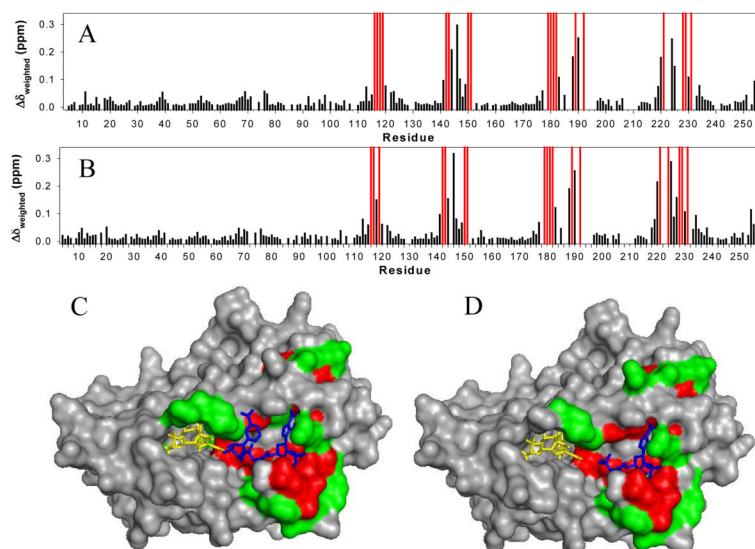


Figure 6.

(A) Per-residue plot of weighted chemical shift perturbations (black lines) obtained upon titration of a solution of *pa*-FPR with a solution of NADP⁺ (A) and with a solution of ADP (B). The weighted values of chemical shift perturbations were obtained from

$$\Delta\delta_{\text{weighted}} = \sqrt{[(\Delta\delta N/5)^2 + \Delta\delta H^2]}/2. \text{ The red lines in the plot correspond to residues whose corresponding cross-peaks decrease in intensity and disappeared during the titration.}$$

(C) Residues whose corresponding cross-peaks exhibited gradual chemical shift perturbations during the titration with NADP⁺ are highlighted green on the surface of the *pa*-FPR-NADP complex, whereas those residues whose cross-peaks decreased in intensity and disappeared during the titration are highlighted in red. FAD and NADP⁺ are rendered in yellow and in blue sticks, respectively. (D) Residues whose cross peaks were affected during the titration of *pa*-FPR with ADP have been highlighted as in (C).

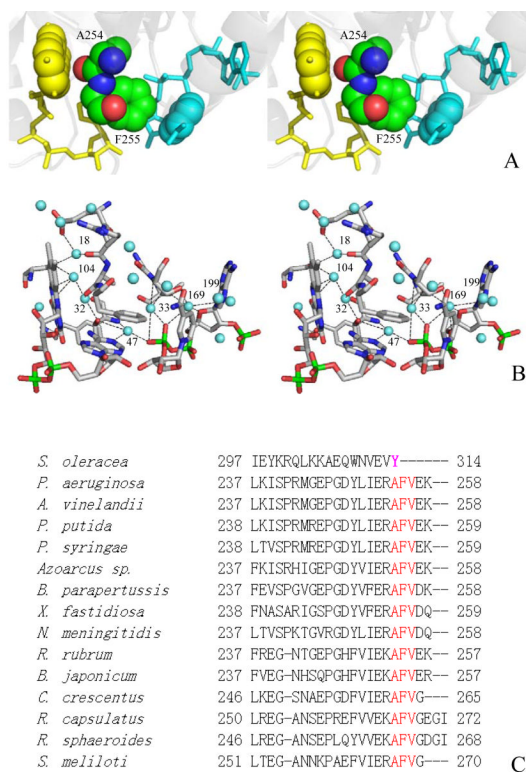


Figure 7.

Stereoviews of (A) possible “electron tunneling path” which starts with the T-stacking of the nicotinamide ring (cyan) and Phe255 aromatic side chain, continues across the peptide bond into Ala255 and across its carbonyl oxygen into the isoalloxazine ring of FAD (yellow). (B) In the context of sequential electron-proton-electron transfer, several structural waters network the nicotinamide and isoalloxazine reactive sites, suggesting a possible path for proton translocation. (C) Amino acid sequence alignment of bacterial subclass I FPR enzymes showing that residues A²⁵⁴, F²⁵⁵ and V²⁵⁶ from the AFVxx motif in the C’-terminal extension are conserved. The C’-terminal sequence of spinach FNR, highlighting the terminal Tyr of plastidic FNRs, is shown for comparison.

Table 1Summary of data collection and structure refinement^a

Data set	FPR(FAD) - NADP ⁺ complex
Space group	P2 ₁ 2 ₁ 2
Unit cell dimensions (Å)	a=67.14 b=73.49 c=51.54 α=β=γ=90°
Protein atoms	2037 [average B-factor = 22.5 Å ²]
Ligands	FAD and NADP ⁺ (101 atoms) [average FAD B-factor = 19.4 Å ²] [average NADP ⁺ B-factor = 24.4 Å ²]
Solvent molecules	288 [average B-factor = 33.1 Å ²]
rmsd ^b bonds (Å)	0.01
rmsd ^b angles (°)	1.7
Resolution range	20–1.90 (1.95–1.90)
Unique reflections	20561 (2895)
Completeness (%)	99.7 (99.4)
I/σI	28.45 (8.44)
R _{merge} (%)	3.8 (15.7)
R _{cryst} ^c (%)	18.1
R _{free} ^d (%)	21.8

^aValues in parentheses refer to the highest-resolution shell.^bRootmean-square deviation from ideal values.^cR_{cryst} = 100 * Σ|F_{obs} - F_{model}| / ΣF_{obs}, where F_{obs} and F_{model} are observed and calculated structure factor amplitudes, respectively.^dR_{free} is the R_{cryst} calculated for randomly chosen unique reflections, which were excluded from the refinement (1234 for FPR liganded with FAD).